2026 IEEE International Conference on Robotics and Automation (ICRA 2026)
June 1-5, 2026. Vienna, Austria

OcTac: An Octopus Sucker-Inspired Vision-Based Tactile Sensor with Self-Adaptive Adhesion

Yi Xiong[1*], Feiyang Yuan[1*], Qiyi Zhang[1], Lei Bao[2] and Li Wen[1]

***Abstract*— Vision-based tactile soft sensors are increasingly applied to robotic perception and manipulation by leveraging high-resolution imaging during contact with environmental surfaces, thereby enabling more adaptable and robust interactions. Nonetheless, ensuring optimal contact force to achieve uniform, conformal, and stable contact between sensors and surfaces remains a key challenge, particularly within complex and unstructured environments. Inspired by the highly versatile suction cups of biological octopuses for environmental surface sensing, we introduce OcTac, a prototype that seamlessly combines adaptive adhesion capabilities with vision-based tactile perception. OcTac harnesses its self-guided adhesion mechanism and the intrinsic flexibility of soft materials to autonomously achieve alignment with target surfaces, even when initially misaligned at significant angles—facilitating tactile perception without relying on precise external control. We conducted experiments demonstrating that OcTac exhibits robust adaptive adhesion and self-detachment capabilities on surfaces with inclination angles ranging from 0° to 90°, as well as on surfaces with varying levels of roughness (with particle sizes up to 150 µm). On challenging inclined surfaces, OcTac's self-aligning adhesion mechanism enables stable and uniform contact, achieving a significant improvement in image uniformity by a factor of 4.53 compared to conventional vision-based tactile soft sensors. Additionally, we demonstrated OcTac mounted on a continuum soft robotic arm, enabling it to navigate around obstacles and perform surface perception, object recognition, and grasping tasks. This work presents a new approach for achieving adaptive tactile perception in complex environments by harnessing the inherent physical intelligence of soft adhesive materials.**

I. Introduction

Achieving dexterous robotic manipulation in unstructured environments critically depends on stable object-surface interactions and the acquisition of comprehensive perceptual data. Vision-based tactile sensors have garnered considerable attention owing to their high-resolution, multi-modal sensing capabilities, and their pivotal role in tasks such as surface inspection [1]–[3] and delicate manipulation [4]–[6]. Their effectiveness hinges on maintaining uniform and stable contact between the soft gel and the target surface [7]. Traditionally mounted rigidly on robotic end-effectors, these sensors necessitate precise perpendicular force application to accurately capture surface topography via gel deformation. In unstructured settings, aligning such sensors with unknown or complex geometries remains a formidable challenge, often resulting in uneven contact forces. This inconsistency compromises tactile image quality and impairs surface reconstruction accuracy, thereby constraining the reliable deployment of vision-based tactile sensing to controlled, simple scenarios. Overcoming these limitations is essential to unlock robust, versatile tactile perception in real-world, unconstrained environments.

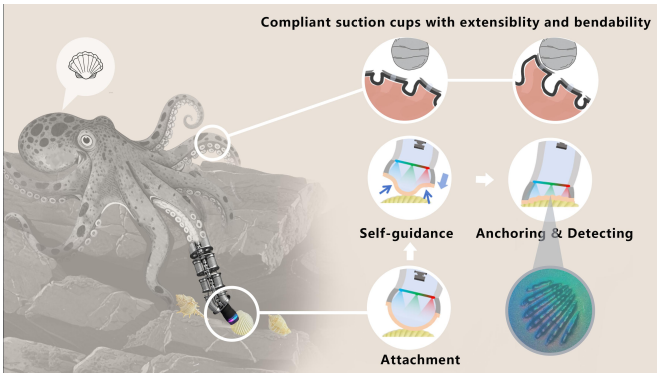

Fig. 1. Overview of OcTac: Octopus has flexible, sensory suction cups. We propose an octopus-inspired suction cup visual tactile sensor OcTac, whose self-guided adhesion characteristics can provide a complete and uniform vision for tactile perception as well as provide new insights for tactile detection in restricted environments.

Suction cups are widely adopted in robotic grasping due to their structural simplicity, low cost, and ease of control. To improve the effectiveness of suction-based manipulation, various sensing modalities have been integrated into suction cup end-effectors, often achieve more accurate and efficient environmental perception via network models. For instance, Dex-Net 3.0 employs a compliant suction contact model together with deep learning to predict seal quality and grasp robustness directly from point clouds [8]. Similarly, end-to-end CNN-based picking systems can infer feasible suction regions in cluttered scenes without explicit object recognition or pose estimation [9]. Despite their effectiveness, these approaches remain strongly dependent on visual observability, and the generalization of data-driven methods in unstructured environments continues to be a significant challenge. To mitigate the failures of purely vision-based planners, several studies have integrated tactile perception into suction cups. Various taitle sensors—including capacitive, strain, and pressure sensors—have been integrated into suction cups [10]–[13]. However, these sensors predominantly capture rudimentary contact information, such as deformation or

*These authors contributed equally to this work.

Corresponding author: Li Wen, E-mail: liwen@buaa.edu.cn

This work was supported by the national Key R&D Program of China (grant nos. 2024YFb4707300 and 2022YFb4701800), and the national Science Foundation support projects, China (grant nos. 62425303, T2121003).

[1]Yi Xiong, Feiyang Yuan, Qiyi Zhang, and Li Wen are with the School of Mechanical Engineering and Automation, Beihang University, Beijing, China.

[2]Lei Bao is with Beijing Soft Robot Tech Co., Ltd., Beijing, China.

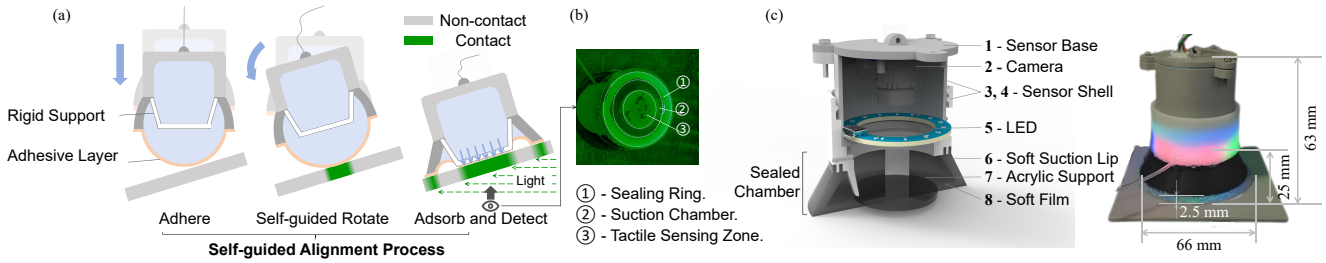

Fig. 2. Design of OcTac. (a) Adhesion self-guided strategy of the suction cup. (b) Bottom view of FTIR experiment. The central region with rigid support ③ serves as the tactile detection zone, while the unsupported peripheral ring area ② collapses inward during adhesion to form the suction chamber. (c) CAD assembly drawing. The component labeled 6 is the soft lip ring cast from silicone. The component labeled 7 is the acrylic rigid support structure fixed to the shell, ensuring effective vision-based tactile perception.

normal force. Smart suction cups [14], [15] utilize internal airflow and pressure measurements to guide haptic exploration, thereby improving grasp robustness. Furthermore, haptically driven grasping strategies have been shown to enhance suction performance on irregular waste PCBs with complex surface-mounted components [16]. However, these sensing modalities primarily capture airflow distributions, offering limited spatial resolution and lacking the capability for dense surface reconstruction. In [17], researchers proposed integrating vision-based tactile sensing within a suction cup. Similaly, however, its primary function was limited to self-posture adjustment rather than detailed perception of external surface topography. As a result, these approaches still depend heavily on external actuators and complex control algorithms to achieve surface alignment. The E-SGAS system [18], featuring an inflatable adhesive membrane and an under-actuated design, can adapt to diverse angles and surface roughness with minimal preload force. Its embedded multi-layer stretchable liquid metal sensing circuitry enables the detection of inflation, contact, adhesion, leakage, and surface roughness. Nevertheless, its sensing capabilities are predominantly oriented toward proprioception, with insufficient spatial resolution and perceptual scope for accurate, high-resolution reconstruction of detailed surface geometries.

The research of vision-tactile sensor after GelSight [19] focuses on miniaturization and higher integration, as demonstrated in [20] and [21]. Leveraging deep learning, vision-based tactile sensors can now perceive textures [22], shapes [23], and extract high-level, multi-modal tactile information such as 6D contact forces [24] and slip detection [25]. A critical prerequisite for effectively deploying these algorithms is maintaining reliable normal contact. Their performance inherently relies on precise pose and force control of external actuators. In scenarios with misaligned or uneven surfaces, low-level tactile signals are prone to distortion or loss, which undermines surface reconstruction quality and diminishes the reliability of tactile perception.

Drawing inspiration from nature, we identify an elegant solution to the surface alignment challenge faced by vision-based tactile sensors. The octopus, a renowned master of dexterous manipulation within complex seabed environments, relies on its arms and suction cups to explore and discriminate objects blindly. Recent studies have demonstrated that octopuses utilize mechano-tactile sensing within their suction cups to distinguish intricate 3D shapes, even in the absence of visual and chemical cues [26]. This remarkable integration of active adhesion and tactile sensing within a compact organ [27] offers valuable insights for robotic design.

Building on this biological principle, we introduce OcTac, an octopus-inspired suction cup prototype that integrates self-guided adhesion with vision-based tactile sensing. OcTac effectively addresses the longstanding challenge of maintaining stable and uniform contact pressure- a task that traditionally requires complex control schemes—particularly in constrained or unstructured environments. This bioinspired design offers a promising avenue for advancing surface inspection and dexterous manipulation in real-world scenarios. By demonstrating a unique synergy between self-guided adhesion and tactile sensing, OcTac enables consistent and reliable tactile detection even under challenging conditions. Beyond endowing the suction cup with high-level tactile perception, this integration enhances the adaptability of vision-based tactile sensors across diverse external environments.

II. Design and Fabrication

A. Design Principles

Inspired by the design of the self-guided suction cup E-SGAS [18], OcTac is designed for attachment, self-alignment, and vision-based tactile perception. The adhesion principle is illustrated in Fig. 2(a). During the preparation phase, positive pressure inflates the suction cup's flexible membrane into a spherical shape, facilitating adaptable contact with the surface. Upon contacting an inclined surface, an initial attachment point is formed. Owing to gravity torque and the compliance of the base connection, the suction cup then rotates to adapt to the slope angle, generating a new attachment point. Because the membrane surface is coated with an adhesive layer, the attachment point is anchored to the surface. Subsequently, negative pressure is applied internally, causing the flexible membrane to rapidly retract inwards. The deformation-induced pulling force guides the suction cup closer to the object surface, forming a seal and completing the adhesion process. Detachment is achieved by reapplying positive pressure to break the seal.

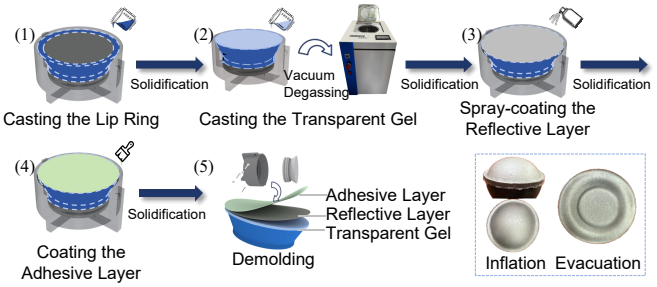

Fig. 3. Fabrication of the Soft Suction Lip. The multilayer structure is fabricated through stepwise casting of silicone with different compositions.

The mechanical structure of OcTac is shown in Fig. 2(c). The assembled prototype has a maximum diameter of approximately 66 mm. We fixed a DX100 camera module with a resolution of 1280×720 to the Sensor Base. To achieve uniform illumination of the tactile sensing area, red, green, and blue LED beads are evenly distributed on a ring-shaped circuit board. OcTac features a sealed chamber, composed of a soft suction lip and an acrylic support, which functions to provide attachment anchoring, self-guided adhesion, and vision-based tactile information representation.

To ensure functional compatibility between vision-based tactile perception and self-guided adhesion, we introduced an acrylic hard support structure fixed to the housing within the airtight chamber. As shown in Fig. 2(b), we built an FTIR (Frustrated Total Internal Reflection) inclined surface system to further illustrate OcTac's operating principle. Because the area of the hard support is smaller than that of the flexible membrane, the central area with support ③ serves as the tactile sensing zone, while the surrounding annular areas ① and ② without support function as the adhesion zones. During adhesion, area ② retracts inwards to form a vacuum chamber, ensuring the adhesive force of the suction cup, while area ① maintains a seal with the target surface. Due to atmospheric pressure, the flexible membrane contacts and presses against the support, generating stable pressure that enables precise vision-based tactile perception.

B. Fabrication of OcTac

The flexible lip ring and flexible membrane were fabricated using a multi-step silicone casting process. Dragon Skin 20 (Smooth-On, USA) silicone, with a Shore Hardness of 20A, was used for the lip, as shown in Fig. 3(1). The membrane, capable of adapting to the different deformation states during inflation and suction of the suction cup, is central to tactile information representation. Parameters of the silicone, such as transparency and hardness, significantly impact the sensing accuracy of the vision-based tactile sensor. As shown in Fig. 3(2), we selected nearly transparent Smooth-On Ecoflex 00-31 Near Clear (Smooth-On, USA), with a Shore Hardness of 00-31, for this casting. After degassing and curing, a reflective metal powder layer was sprayed onto the membrane to enhance reflectivity, as shown in Fig. 3(3). To enable the self-guided adhesion mechanism, an adhesive layer was needed. Notably, an overly thick adhesive layer impairs texture perception. The highly deformable adhesive material fills surface gaps upon contact, which restricts deformation of the underlying reflective layer and thus obscures fine textural details. Therefore, the adhesive layer was prepared by mixing metal powder, stretchable adhesive silicone (Dreamink, China), and a diluent at a mass ratio of 1:20:20, as shown in Fig. 3(4), to achieve a balance between tackiness and surface texture capture.

C. 3D Reconstruction Method

The key to reconstructing the geometric features of the contact surface lies in extracting surface depth information from the captured BGR images under known lighting conditions. We utilized tricolor (BGR) light sources to illuminate the silicone body from different directions. After deformation during adhesion, the surface exhibits distinct brightness variations. Based on this, the surface gradient can be recovered from the images, and the local depth can be solved through integration. Specifically, according to the Lambert reflectance model, light incident on a surface produces diffuse reflection. The observed intensity (grayscale value) at a point is proportional only to the cosine of the angle between the incident light direction and the surface normal at that point, i.e.:

$$L_c = \lambda \cdot I \cdot \max(0, \vec{n} \cdot \vec{s_c}) \tag{1}$$

where L_c is the grayscale value at a point in the field of view, I is the incident light intensity, $\vec{n}$ is the normal vector of the contact surface, $\vec{s_c}$ is the incident light vector, the max function ensures non-negativity of the result, and λ is a coefficient related to the material's reflective properties.

Following the Lambert reflectance model, the corresponding observed grayscale values for the three channels are:

$$\begin{cases} L_B = \lambda \cdot I_B \cdot \sum_{i=1}^{5} \max(0, \vec{n} \cdot \vec{s_i}) \\ L_G = \lambda \cdot I_G \cdot \sum_{j=1}^{5} \max(0, \vec{n} \cdot \vec{s_j}) \\ L_R = \lambda \cdot I_R \cdot \sum_{k=1}^{5} \max(0, \vec{n} \cdot \vec{s_k}) \end{cases} \tag{2}$$

where L_B, L_G, and L_R represent the observed grayscale values for the B, G, and R channels, respectively; I_B, I_G, and I_R represent the light intensities of the B, G, and R sources.

There are five point sources of each color. The light direction vector from each individual point source to the observation point is unique. These vectors are denoted as $\vec{s_i}$, $\vec{s_j}$, and $\vec{s_k}$ for the blue, green, and red sources, respectively. Therefore, the grayscale value for a single color channel is expressed as the sum of the dot products of the surface normal vector $\vec{n}$ at the observation point and the direction vectors of all point sources of that color, multiplied by the diffuse reflection coefficient λ and the light intensity $I_{B/G/R}$. We assume that the reflective layer is uniform and the gray

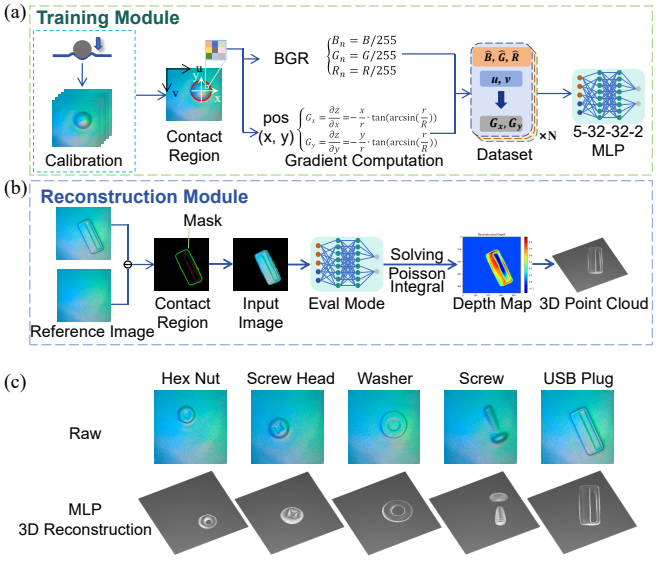

Fig. 4. Surface reconstruction algorithm. (a) Flow chart of the training module. The MLP model is trained using an image of a spherical indentation (diameter 10 mm). (b) Flow chart of reconstruction module. The trained MLP model is used to predict the gradient of the contact region, and the depth map is reconstructed by solving Poisson integral. (c) Reconstruction results of typical objects.

coating exhibits consistent absorption rates for B, G, and R light, the diffuse reflection coefficient λ is consequently the same for all three channels.

According to [28], for a given point in the field of view with fixed light source directions $\vec{s}$, a functional relationship exists between the tricolor grayscale values and the normal vector $\vec{n}$ of the contact surface at that point, denoted here as:

$$L(x, y) = f[\vec{n}(x, y)] \tag{3}$$

where (x, y) represent the point's position.

The surface gradient can be further derived from the normal vector. Consequently, a relationship between the grayscale values and the surface gradient can be established, denoted as:

$$L(x, y) = g[G_x(x, y), G_y(x, y)] \tag{4}$$

Here, G_x and G_y represent the gradients in the x and y directions, respectively. The surface depth z and the gradient field satisfy:

$$\begin{cases} G_x = \dfrac{\partial z}{\partial x} \\ G_y = \dfrac{\partial z}{\partial y} \end{cases} \tag{5}$$

A Poisson equation is constructed,

$$\nabla^2 z = \mathrm{div}(G_x, G_y) = \frac{\partial G_x}{\partial x} + \frac{\partial G_y}{\partial y} \tag{6}$$

where $\mathrm{div}(Gx, Gy)$ denotes the divergence operator.

Therefore, by mapping the tricolor (BGR) pixel values of the contact area to the surface gradient, the surface depth can be reconstructed using an integration solver.

Based on the above derivation, we trained an MLP (Multilayer Perceptron) model to map the BGR values of the contact area to the gradients (G_x, G_y). As shown in Fig. 4(a), a 10 mm diameter sphere was pressed against the sensor at different locations. The contact regions were extracted. For each pixel within these regions, its normalized BGR values were paired with the gradient values calculated based on the known spherical geometry. In total, 85 contact images were collected, resulting in about 2 million valid pixel samples. The normalized BGR values and pixel coordinates (u, v) were used as input features, and the gradient values G_x, G_y served as output labels, to form the dataset [29]. The dataset was randomly divided into training and validation sets with a ratio of 8:2. The MLP comprised three fully connected hidden layers with 32 neurons each and $Tanh$ activation functions. The trained MLP network can infer the gradient field for objects of unknown geometry.

The divergence term was computed using second-order central finite differences. The Poisson equation was discretized on a regular grid and solved iteratively via the Gauss–Seidel method. Consequently, the depth map can be reconstructed as shown in Fig. 4(b). The reconstruction results for some typical objects are shown in Fig. 4(c).

III. Experiment and Results

A. Mechanical Evaluation

To evaluate OcTac's mechanical performance, we tested its adhesion and detachment forces. The experimental setup consisted of a robotic arm (AUBO, China), a six-axis force sensor (DECENT, China), and a pneumatic control system. An acrylic plate was fixed to an optical table to serve as the test surface. The suction cup was connected to the force sensor attached to the robotic arm's end flange via a cord. The robotic arm was programmed to control the descent and ascent of the suction cup, while the normal force was monitored in real-time.

For the adhesion test, the suction cup descended at 0 kPa until contact, then negative pressure was triggered. The arm then lifted the suction cup vertically until detachment, to measure the adhesive force. Pressure was increased from −2 kPa to −30 kPa in 2 kPa increments. As shown in Fig. 5(a), adhesion force increased approximately linearly with negative pressure, from 12.484 N at 0 kPa to 54.079 N at −30 kPa. The results show that within the range of 0 to −30 kPa, the measured adhesion force exceeds the force attributable solely to the applied negative pressure (gray dashed line).

For the detachment test, the suction cup was initially adhered at −30 kPa. Positive pressure was then applied, and the arm lifted the suction cup. The detachment force decreased sharply as positive pressure rose. At 3 kPa, the force dropped to 2.366 N, representing an 83.30% reduction compared to the initial value. With positive pressure further increased to 5 kPa, the detachment force measured only

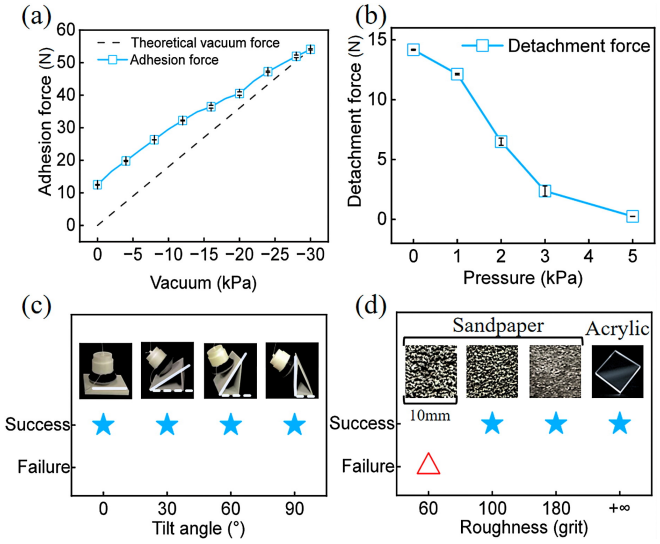

Fig. 5. Adhesion performance of OcTac. (a) Negative pressure vs. adhesion force characteristic curve. The blue line for adhesion force and the gray dashed line for theoretical negative pressure force. (b) Positive pressure vs. detachment force characteristic curve. (c) Self-adaptive adhesion capability on inclined surfaces with varying tilt angles. (d) Adhesion performance on surfaces with different roughness levels.

0.248 N, equivalent to 1.75% of the initial force. These results confirm that the suction cup's outward expansion mechanism enables reliable and efficient active detachment.

B. Adaptive Evaluation

To evaluate the adhesion adaptability of OcTac to surfaces with different inclination angles, we tested the suction cup's adhesion performance at 0°, 30°, 60°, and 90°. Experiments were conducted under an initial condition of 2 kPa and an adhesion condition of −20 kPa. As shown in Fig. 5(c), results demonstrate that the suction cup successfully achieved adhesion in all cases (from 0° to 90°). Therefore, OcTac's adaptability to different inclined surfaces reduces the positioning accuracy requirements for the carrying platform.

To evaluate OcTac's adhesion adaptability to surfaces with different roughness levels, we selected four surfaces with varying roughness: 60-grit, 100-grit, 180-grit sandpaper, and near-smooth acrylic, and performed the roughness adaptability test. The sandpapers were attached to identical acrylic plates (100 mm × 100 mm × 2 mm), ensuring that all other experimental conditions remained consistent across tests. Each acrylic plate had a mass of 24 g, while the mass contribution of the sandpaper layer was negligible. Under an initial positive pressure of 2 kPa, the flexible membrane of the suction cup bulged. Adhesion was initiated immediately upon contact with the test surface, ensuring nearly minimal preload force. For the smooth acrylic surface and the 100-grit sandpaper surface, the suction cup successfully achieved adhesion at −20 kPa. However, the adhesion failed when the roughness increased to 60-grit, as shown in Fig. 5(d). This is because the surface particle size was too large (250 µm), preventing the flexible membrane from completely filling the microscopic gaps in the contact surface, thus compromising the seal. The experimental results show that this suction cup has a degree of adaptability to different surface roughness levels. With a very small preload, the successful adhesion range extends from smooth surfaces to those with the particle size larger than 150 µm. However, to adhere to rougher surfaces, a larger preload force is required to enable the sticky material to fill the gaps and ensure the airtightness of the vacuum chamber.

C. Surface Detection Experiments

For vision-based tactile perception, alignment is a critical step. Conventional GelSight-like sensors rely on externally applied normal force, which often results in uneven contact pressure, particularly on inclined or uneven surfaces. This leads to distortion or even loss of tactile information. To evaluate the impact of OcTac's active adhesion characteristics on this process, we conducted a dot array detection experiment on an inclined surface.

We designed a 30° inclined surface featuring a dot array with 2 mm diameter, 0.35 mm height, and 3 mm spacing as the detection target. OcTac was connected via a cord to a winch mounted at the base of a soft robotic arm (SRT, China). The winch, driven by a stepper motor, controlled the winding and unwinding of the cord. This setup enabled a switch between rigid and soft connection at the arm-suction cup interface: tightening the cord locked the cup to the arm's end, while loosening it allowed the cup to freely adjust its posture and achieve alignment with the target surface through self-guided adhesion.

First, with the cord tightened and OcTac fixed to the arm's end, the soft arm was driven to approach and attempt to align with the target surface. In this attempt, OcTac was not activated, functioning like a typical vision-based tactile sensor that acquires tactile information through passive squeezing. After squeezing against the target surface, the resulting tactile image showed dots of varying sizes and an incomplete array due to uneven force distribution, as shown in Fig. 6(a). Subsequently, we loosened the cord, allowing OcTac to attach to the target surface. Negative pressure was then applied to achieve adhesion, providing a uniform and stable contact force for tactile detection. The dot array appeared complete and uniform in the field of view, as shown in Fig. 6(b). By processing the tactile images, we obtained the mean width and standard deviation of the dots under both alignment methods, shown in Fig. 6(c). The deviation of the mean width from a standard value indicates the accuracy of tactile perception, while the error bars represent its uniformity. The results show that compared to the passive alignment method, active adhesion improves tactile perception uniformity by a factor of 4.53 (calculated as the ratio of the standard deviations).

Furthermore, we varied the negative pressure applied to OcTac during adhesion (from −1 kPa to −15 kPa) to observe its effect on tactile detection. Specifically, we extracted the widths of the dots in the field of view from the tactile images. For the dots in rows 1, 3, and 5, we calculated their mean widths (denoted as W_1, W_3, W_5) and plotted the change in

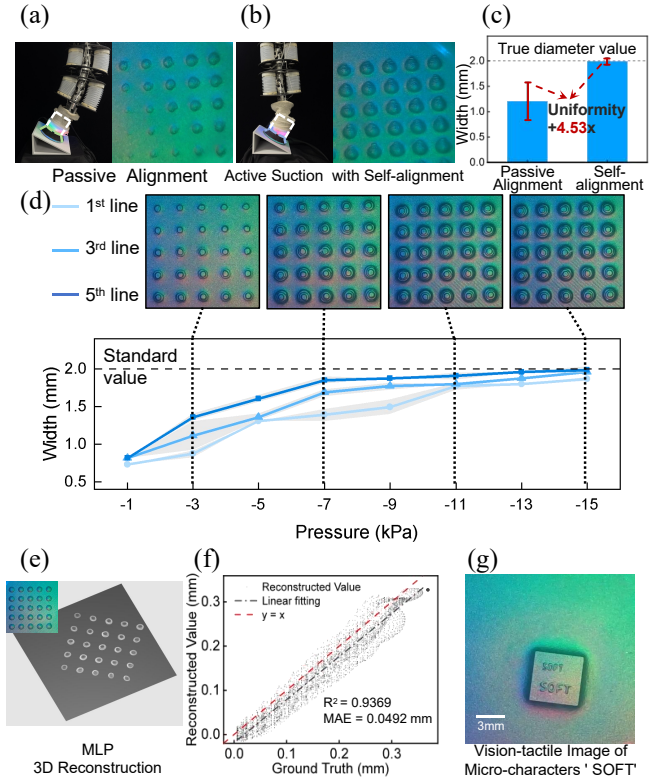

Fig. 6. Verification of the improvement of tactile perception quality by the uniform normal pressure provided by the suction cup. (a) Passive extrusion using the soft arm only. Due to uneven contact force distribution, the dot array appears incomplete and exhibits significant variation in dot size. (b) Active suction-assisted tactile perception. The suction cup provides a more uniform normal pressure, resulting in a complete and consistent dot array. (c) Comparison of the mean dot width and its standard deviation under the two alignment strategies. The dashed line indicates the true dot diameter(2 mm). Contact uniformity is defined as the standard deviation of the dot width distribution. Active adhesion reduces the standard deviation by a factor of 4.53 compared to passive extrusion. (d) Tactile detection of target surface by OcTac under different negative pressures, illustrating the effect of suction pressure on contact stability and uniformity. (e) 3D reconstruction results of circular dot array. (f) Scatter plot of the reconstructed depth values against the ground truth values. (g) Micro-characters detection.

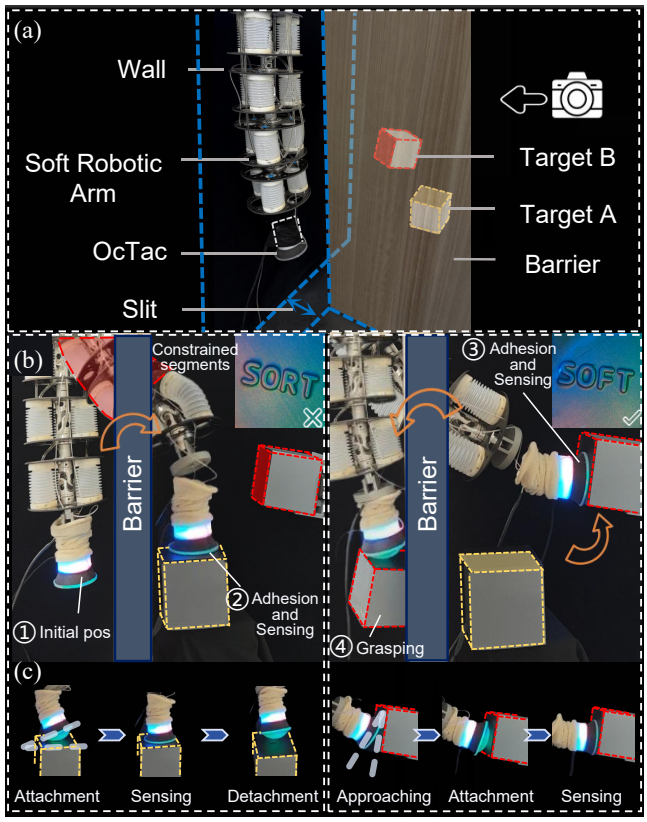

Fig. 7. Perception and grasping in a narrow slit. (a) Schematic of the experimental setup, showing the narrow slit formed by walls and obstacles, and the two target objects (A: yellow block with "SORT"; B: red block with "SOFT"). (b) Sequence of the overall experimental procedure, demonstrating the soft arm carrying OcTac navigating through the slit, performing tactile sensing on targets A and B sequentially, and successfully grasping target B. (c) The self-guided adhesion, tactile perception processes on the top surface of target A and the side surface of target B.

these means with increasing negative pressure, as shown in Fig. 6(d). As the negative pressure increased, W_1, W_3, and W_5 all showed an upward trend, indicating that a stronger adhesive force resulted in a greater indentation depth. When the negative pressure exceeded −9 kPa, the growth rate of the mean widths slowed, suggesting that the indentation depth was approaching its maximum. At this point, the reconstruction of the target surface was more complete compared to conditions with lower negative pressure (less than −9 kPa). Additionally, we calculated the range (difference between the maximum and minimum values) of the dot widths. A smaller range indicates more uniform pressure distribution and better detection performance. The results showed that the range ΔW decreased significantly after reaching −9 kPa, indicating more uniform pressure distribution under higher negative pressure.

We performed a 3D reconstruction of the dot array surface, with the results shown in Fig. 6(e). Fig. 6(f) presents a scatter plot of the reconstructed depth values against the ground truth values for all valid pixels, showing a highly linear distribution. A trend line fitted to the data points aligns well with the ideal line $y = x$. However, a slightly lower constant term in the fit might originate from manufacturing errors in the dot array sample itself.

To further validate OcTac's capability in resolving fine surface topography, we fabricate a surface with micro-characters, where each letter is approximately 0.5 mm in size. As shown in Fig. 6(g), the tactile image from OcTac is able to clearly resolve and distinguish these characters.

D. Perception and Grasping in a Constrained Space

The aforementioned experiments have demonstrated that OcTac's active self-alignment enables uniform and stable tactile measurements. To further validate its performance in constrained environments, we controlled the soft robotic arm to navigate through a narrow slit formed by walls and obstacles to perform adhesive sensing on two targets, A and B, placed in different poses. The goal was to grasp target B, marked "SOFT", and avoid target A, marked "SORT".

For the first object (the yellow block in Fig. 7(a)), we

detected its top surface and determined it was not the target intended for grasping. Consequently, positive pressure was applied to OcTac to achieve detachment. For target B (the red block), we detected its side surface. After confirming the correct character was present, the object was grasped and extracted from the slit. The entire process is shown in Fig. 7(b) and the supplementary video.

After navigating through the slit, the motion of the proximal segments of the soft arm was constrained, complicating alignment. As can be seen in Fig. 7(c), an angle existed between OcTac and the surface initially. However, it successfully utilized its self-guided adhesion to pull itself toward the target surface and complete the adhesion. Achieving a seal with the top surface of target A was relatively straightforward due to gravity. However, the sensing area for target B was on its side, demonstrating that OcTac's self-guided adhesion capability, aided by adhesive forces, can overcome gravitational effects to some extent.

Our task requires character recognition, so complete tactile perception is important. Before adhesion, uneven pressure resulted in incomplete word images, hindering identification. After adhesion with negative pressure, the words became clear and identifiable. Therefore, this experiment verifies that OcTac can achieve reliable high-resolution tactile perception under constrained conditions, and provides new insights into the problem that it is difficult for a manipulator or dexterous hand to provide a stable normal contact force for tactile detection in constrained environments.

IV. CONCLUSIONS

This paper presents OcTac, an octopus-inspired suction cup prototype that enhances vision-based tactile perception. The core contribution of OcTac lies in its ability to adaptively align with target surfaces by leveraging its self-guided adhesion capability, thereby providing a uniform and stable field of view for vision-based tactile sensing. This strategy ensures a uniform pressure distribution across the gel layer upon contact with the target surface, significantly reducing the dependence on precise external control.

Experiments that OcTac's remarkable adaptability to surfaces with various inclination angles of 0-90° and roughness of up to 100-grit. The dot array detection experiment conducted on an inclined surface shows that, compared to passive alignment methods, OcTac's active adhesion capability enables a 4.53-fold increase in uniformity and more accurate tactile measurements. Furthermore, the grasping experiment within a confined slit demonstrate OcTac's ability to recognize surface features based on tactile information and successfully identify and manipulate the target object, highlighting its potential for application in unstructured environments.

ACKNOWLEDGMENT

This work was supported by the national Key R&D Program of China (grant nos. 2024YFb4707300 and 2022YFb4701800), and the national Science Foundation support projects, China (grant nos. 62425303, T2121003).

REFERENCES

[1] H. Kim, O. C. Kara, and F. Alambeigi, "A soft and inflatable vision-based tactile sensor for inspection of constrained and confined spaces," *IEEE Sensors Journal*, vol. 23, no. 23, pp. 29605–29618, 2023.

[2] M. A. Mirzaee, H.-J. Huang, and W. Yuan, "Gelbelt: a vision-based tactile sensor for continuous sensing of large surfaces," *IEEE Robotics and Automation Letters*, 2025.

[3] A. Böhm, T. Schneider, B. Belousov, A. Kshirsagar, L. Lin, K. Doerschner, K. Drewing, C. A. Rothkopf, and J. Peters, "What matters for active texture recognition with vision-based tactile sensors," in *2024 IEEE International Conference on Robotics and Automation (ICRA)*, pp. 15099–15105, IEEE, 2024.

[4] M. Lambeta, P.-W. Chou, S. Tian, B. Yang, B. Maloon, V. R. Most, D. Stroud, R. Santos, A. Byagowi, G. Kammerer, *et al.*, "Digit: A novel design for a low-cost compact high-resolution tactile sensor with application to in-hand manipulation," *IEEE Robotics and Automation Letters*, vol. 5, no. 3, pp. 3838–3845, 2020.

[5] J. Xu, L. Wu, C. Lin, D. Zhao, and H. Xu, "Dtactive: A vision-based tactile sensor with active surface," *arXiv preprint arXiv:2410.08337*, 2024.

[6] I. Andrussow, H. Sun, K. J. Kuchenbecker, and G. Martius, "Minsight: A fingertip-sized vision-based tactile sensor for robotic manipulation," *Advanced Intelligent Systems*, vol. 5, no. 8, p. 2300042, 2023.

[7] Z. Zou, Z. Li, Y. Zhou, G. Zhou, W. Xu, W. Wu, H. Zhang, Z. Chen, Z. Dai, and X. Li, "Monitoring soft shape surface deformation via optical images for the distinction of contact state," *Advanced Intelligent Systems*, vol. 6, no. 3, p. 2300535, 2024.

[8] J. Mahler, M. Matl, X. Liu, A. Li, D. Gealy, and K. Goldberg, "Dex-net 3.0: Computing robust vacuum suction grasp targets in point clouds using a new analytic model and deep learning," in *2018 IEEE International Conference on robotics and automation (ICRA)*, pp. 5620–5627, IEEE, 2018.

[9] Q. Shao, J. Hu, W. Wang, Y. Fang, W. Liu, J. Qi, and J. Ma, "Suction grasp region prediction using self-supervised learning for object picking in dense clutter," in *2019 IEEE 5th International Conference on Mechatronics System and Robots (ICMSR)*, pp. 7–12, IEEE, 2019.

[10] S. Doi, H. Koga, T. Seki, and Y. Okuno, "Novel proximity sensor for realizing tactile sense in suction cups," in *2020 IEEE International Conference on Robotics and Automation (ICRA)*, pp. 638–643, IEEE, 2020.

[11] E. Shahabi, F. Visentin, A. Mondini, and B. Mazzolai, "Octopus-inspired suction cups with embedded strain sensors for object recognition," *Advanced Intelligent Systems*, vol. 5, no. 2, p. 2200201, 2023.

[12] Z. Wang, G. Sun, X. Fan, P. Xiao, and L. Zhu, "Biomimetic octopus suction cup with attachment force self-sensing capability for cardiac adhesion," *Soft Robotics*, vol. 11, no. 6, pp. 1043–1054, 2024.

[13] S. Aoyagi, M. Suzuki, T. Morita, T. Takahashi, and H. Takise, "Bellows suction cup equipped with force sensing ability by direct coating thin-film resistor for vacuum type robotic hand," *IEEE/ASME Transactions on Mechatronics*, vol. 25, no. 5, pp. 2501–2512, 2020.

[14] T. M. Huh, K. Sanders, M. Danielczuk, M. Li, Y. Chen, K. Goldberg, and H. S. Stuart, "A multi-chamber smart suction cup for adaptive gripping and haptic exploration," in *2021 IEEE/RSJ international conference on intelligent robots and systems (IROS)*, pp. 1786–1793, IEEE, 2021.

[15] J. Lee, S. D. Lee, T. M. Huh, and H. S. Stuart, "Haptic search with the smart suction cup on adversarial objects," *IEEE Transactions on Robotics*, vol. 40, pp. 226–239, 2023.

[16] J. Lee, Z. Sun, Z. Dong, F. Chen, and H. S. Stuart, "Regrasping on printed circuit boards with the smart suction cup," in *2024 IEEE International Conference on Robotics and Automation (ICRA)*, pp. 6477–6483, IEEE, 2024.

[17] S. van Veggel, M. Wiertlewski, E. L. Doubrovski, A. Kooijman, B. Mazzolai, and R. B. Scharff, "Optoelectronically innervated suction cup inspired by the octopus," *Advanced Intelligent Systems*, vol. 7, no. 4, p. 2400544, 2025.

[18] F. Yuan, L. Tian, H. Xu, Z. Fu, W. Wu, Z. Xie, B. Yuan, T. Wang, X. Ding, and L. Wen, "A sensorized mechanically self-guided suction cup for improved adhesion in complex environments," *Soft Robotics*, 2025.

[19] W. Yuan, S. Dong, and E. H. Adelson, "Gelsight: High-resolution robot tactile sensors for estimating geometry and force," *Sensors*, vol. 17, no. 12, p. 2762, 2017.

[20] A. Padmanabha, F. Ebert, S. Tian, R. Calandra, C. Finn, and S. Levine, "Omnitact: A multi-directional high-resolution touch sensor," in *2020 IEEE International Conference on Robotics and Automation (ICRA)*, pp. 618–624, IEEE, 2020.

[21] D. F. Gomes, Z. Lin, and S. Luo, "Geltip: A finger-shaped optical tactile sensor for robotic manipulation," in *2020 IEEE/RSJ international conference on intelligent robots and systems (IROS)*, pp. 9903–9909, IEEE, 2020.

[22] S. Luo, W. Yuan, E. Adelson, A. G. Cohn, and R. Fuentes, "Vitac: Feature sharing between vision and tactile sensing for cloth texture recognition," in *2018 IEEE International Conference on Robotics and Automation (ICRA)*, pp. 2722–2727, IEEE, 2018.

[23] W. Xu, Z. Yu, H. Xue, R. Ye, S. Yao, and C. Lu, "Visual-tactile sensing for in-hand object reconstruction," in *Proceedings of the IEEE/CVF conference on computer vision and pattern recognition*, pp. 8803–8812, 2023.

[24] C. Lin, H. Zhang, J. Xu, L. Wu, and H. Xu, "9dtact: A compact vision-based tactile sensor for accurate 3d shape reconstruction and generalizable 6d force estimation," *IEEE Robotics and Automation Letters*, vol. 9, no. 2, pp. 923–930, 2023.

[25] J. Li, S. Dong, and E. Adelson, "Slip detection with combined tactile and visual information," in *2018 IEEE International Conference on Robotics and Automation (ICRA)*, pp. 7772–7777, IEEE, 2018.

[26] K. C. Buresch, N. D. Huget, W. C. Brister, E. Y. Zhou, A. S. Lineaweaver, C. Rifai, J. Hu, Z. E. Stevenson, J. G. Boal, and R. T. Hanlon, "Evidence for tactile 3d shape discrimination by octopus," *Journal of Comparative Physiology A*, vol. 210, no. 5, pp. 815–823, 2024.

[27] S. van Veggel, M. Wiertlewski, E. L. Doubrovski, A. Kooijman, E. Shahabi, B. Mazzolai, and R. B. Scharff, "Classification and evaluation of octopus-inspired suction cups for soft continuum robots," *Advanced Science*, vol. 11, no. 30, p. 2400806, 2024.

[28] S. Zhang, Y. Yang, Y. Sun, N. Liu, F. Sun, and B. Fang, "Artificial skin based on visuo-tactile sensing for 3d shape reconstruction: Material, method, and evaluation," *Advanced Functional Materials*, vol. 35, no. 1, p. 2411686, 2025.

[29] S. Wang, Y. She, B. Romero, and E. Adelson, "Gelsight wedge: Measuring high-resolution 3d contact geometry with a compact robot finger," in *2021 IEEE International Conference on Robotics and Automation (ICRA)*, pp. 6468–6475, IEEE, 2021.